Atmos. Chem. Phys., 24, 2937–2950, 2024
https://doi.org/10.5194/acp-24-2937-2024

Atmospheric Chemistry and Physics
Open Access
EGU

Measurement report: Water diffusion in single suspended phase-separated aerosols

Yu-Kai Tong[1,2], Zhijun Wu[3], Min Hu[3], and Anpei Ye[1]

[1]Key Laboratory for the Physics and Chemistry of Nanodevices, School of Electronics, Peking University, Beijing 100871, China
[2]School of Physics and Institute for Advanced Study in Physics, Zhejiang University, Hangzhou 310027, China
[3]State Key Joint Laboratory of Environmental Simulation and Pollution Control, College of Environmental Sciences and Engineering, Peking University, Beijing 100871, China

Correspondence: Anpei Ye (yap@pku.edu.cn)

Received: 20 June 2023 – Discussion started: 12 July 2023
Revised: 29 November 2023 – Accepted: 25 December 2023 – Published: 7 March 2024

Abstract. Water diffusion is a typical thermodynamic process in ambient aerosols that plays pivotal roles in their physicochemical properties and atmospheric lifetime and influences the climate and human health. A fair amount of aerosols become phase-separated after experiencing atmospheric aging processes such as efflorescence, amorphization, and liquid–liquid phase separation. However, detecting the hygroscopicity of heterogeneous aerosols is quite intractable. Here, for the first time, we directly characterized the water diffusion in single suspended phase-separated aerosols via a self-constructed laser tweezer Raman spectroscopy (LTRS) system. The H_2O–D_2O isotope exchange was harnessed to trace the water diffusion in single laser-levitated homogenous/heterogeneous microdroplets. The time-resolved cavity-enhanced Raman spectra of the microdroplets were used to detect the diffusion process in real time. Two archetypes of phase-separated aerosols, i.e., partially engulfed and core–shell, were studied. Moreover, we quantified the dynamic water diffusion process by experimentally measuring the diffusion coefficients. The results showed that compared with the homogenous aerosols, water diffusion limitations existed in the phase-separated aerosols. The incomplete diffusion may stem from the formation of certain hydrated molecule clusters. This work provides possible implications for the evolutions, especially the gas–particle partition, of the actual phase-separated atmospheric aerosols.

1 Introduction

Gas–particle partitioning is one of the most significant atmospheric processes of aerosols and plays a crucial role in impacting air quality and the atmospheric environment. As water is often the most mobile component in troposphere aerosols, a clear picture of water diffusion within aerosols is essential. Under various meteorological conditions, the size and refractive index of aerosols change via hydration and dehydration, which then influence the optical properties and ice-nucleating ability of aerosols and the atmospheric energy distribution (Hallquist et al., 2009; Mellouki et al., 2015; Titos et al., 2016). Moreover, water diffusion dictates the moisture content in aerosols and then impacts their component concentrations and phase states. Some previous works have shown that a substantial fraction of secondary organic aerosols (SOAs) have glassy or gel states which present slow heterogeneous reaction rates and nonequilibrium gas–particle partition (Bones et al., 2012; Fowler et al., 2020; Shiraiwa and Pöschl, 2021). It then may lead to significant kinetic constraints on aerosol processing, heterogeneous chemistry, and component lifetimes (Renbaum-Wolff et al., 2013a; Shiraiwa et al., 2011; Vaden et al., 2011).

Numerous techniques have been developed to study the hygroscopicity of aerosols, including electrodynamic balance, a humidified tandem differential mobility analyzer, micro-Fourier transform infrared (FTIR) spectroscopy, atomic force microscopy, X-ray elemental microanalysis, and attenuated total reflection FTIR spectroscopy (Kreiden-

weis and Asa-Awuku, 2014; Tang et al., 2019; Kuang et al., 2020). In these techniques, four main methods are used to detect the water diffusion process. (i) The differential step isothermal method developed by (Aristov et al., 2006; Cai et al., 2015; Lv et al., 2020; Tong et al., 2022a, b) circumvents the non-linear boundary value problem in analyzing the water diffusion process and can readily retrieve the water diffusion coefficient by fitting the response of a single droplet to a changing relative humidity (RH) during sorption/desorption experiments. However, it can only be used to simulate the hygroscopic process of high-viscosity droplets where water diffusion is quite slow and cannot apply to constant-RH conditions. (ii) The Stokes–Einstein (S–E) equation relates the water diffusion coefficient to the particle viscosity. Many experimental and theoretic evaluation methods have been developed to measure the viscosity of aerosol particles both in the laboratory and in the field (Sastri and Rao, 1992; Cao et al., 1993; Rothfuss and Petters, 2017; Booth et al., 2014; Maclean et al., 2021; Smith et al., 2021; Fitzgerald et al., 2016; Renbaum-Wolff et al., 2013b; Bishop et al., 2004). However, application of the S–E equation in tandem with viscosity measurements may also miscalculate the diffusion coefficient because the S–E equation has been shown to break drown at high viscosities (Power et al., 2013; Molinero and Goddard, 2005). (iii) Another method leverages the response of aerosols to the oscillating RH to retrieve the diffusion coefficient. The exploited RH is regulated to oscillate in pulse form (Leng et al., 2015; Shi et al., 2017) or sinusoidal form (Preston et al., 2017) . For a sinusoidal RH oscillation, the amplitude and frequency of the aerosol size fluctuation are dictated by the RH frequency and the diffusion coefficient of water molecules. Nonetheless, this method demands a highly sensitive and precise RH control system, which increases the complexity of the experiments. (iv) The isotopic tracer method can directly unveil the water diffusion process of aerosol droplets, where the deuterium oxide (D_2O) molecules are leveraged to trace the diffusion of water within hydrogen oxide (H_2O) microdroplets (Price et al., 2014; Davies and Wilson, 2016; Moridnejad and Preston, 2016; Nadler et al., 2019). One prominent advantage of this method is that it is able to study the water diffusion process under constant-RH conditions, where the chief driving force of diffusion is the concentration gradient rather than RH changes, while the aforementioned methods can only study the hygroscopic response of aerosols to RH changes.

Previous works have mainly focused on the hydration/dehydration of homogenous aerosols. However, a plethora of studies have shown that phase separation is prevalent in ambient aerosols (You et al., 2014; Freedman, 2017, 2020; Pöhlker et al., 2012; You et al., 2012; Lee et al., 2020). Modeling works show that ignoring phase separation by forcing a single non-ideal phase can lead to vastly incorrect gas–particle partitioning predictions (Pye et al., 2017; Zuend and Seinfeld, 2012). Indeed, it is now widely recognized that the existence of heterogeneous states (e.g., phase-separated and amorphous states) could have significant consequences for the composition of the condensed aerosol phase. For example, the isoprene-derived SOAs are typical phase-separated aerosols which are formed by heterogeneous reactive uptake of epoxydiols onto sulfate aerosol particles. Some works reported that the growth of SOA coatings may impede the reactive uptake of epoxydiols, rendering a self-limiting effect in isoprene-derived SOA formation (Zhang et al., 2018, 2019; Riva et al., 2019). A similar diffusion limitation was also observed in the uptake of α-pinene oxide onto acidic aerosols (Drozd et al., 2013) and in the ozonolysis of polycyclic aromatic hydrocarbons within SOAs (Zhou et al., 2019). For water diffusion, the reported results were inconsistent. Davies et al. (2013) found that organic coatings (long-chain alcohols) may reduce the evaporation of the aerosol liquid water and enhance the condensation of water on the droplets. Other works found that the water condensation was hampered by organic shells and that the hygroscopic growth of phase-separated aerosols was dependent on the thickness of the shells (Ruehl and Wilson, 2014; Li et al., 2021; Mikhailov et al., 2021). However, some other works reported that phase separation had no profound effect on water diffusion under normal ambient conditions (Chan et al., 2006; Zawadowicz et al., 2015; Lienhard et al., 2015).

Notwithstanding, nearly all previous works used the substrate-deposited samples to study mass transfer in phase-separated aerosols. Contrastingly, contactless single particle techniques are appealing because the impacts of surface perturbations on component concentrations and aerosol morphology can be excluded (Zhou et al., 2014). In addition, single particle measurements are preferred over ensemble-averaged experiments because composition and local chemical environments vary from particle to particle. In this work, we utilized isotope tracing to characterize the water diffusion process in single suspended phase-separated aerosols at constant RH and room temperature via a self-constructed laser tweezer Raman spectroscopy (LTRS) system. The time-resolved cavity-enhanced Raman spectra of the microdroplets were recorded to both detect the phase state and reveal the diffusion of water. Three types of aerosols are studied herein, including homogenous aerosols (D_2O + citric acid (CA)), partially engulfed aerosols (H_2O + ammonium sulfate (AS) + oleic acid (OA)), and core–shell aerosols (H_2O + AS + diethyl-L-tartrate (DLT) and H_2O + AS + 1,2,6-hexanetriol (HEX)). Moreover, the influence of acid on water diffusion in aerosols are also discussed.

2 Experiments and methods

2.1 Laser tweezer Raman spectroscopy system

A schematic of the LTRS system is shown in Fig. 1. A laser beam with a wavelength of 532 nm (Excelsior-532-200, Spectra-Physics) was used as both a Raman-

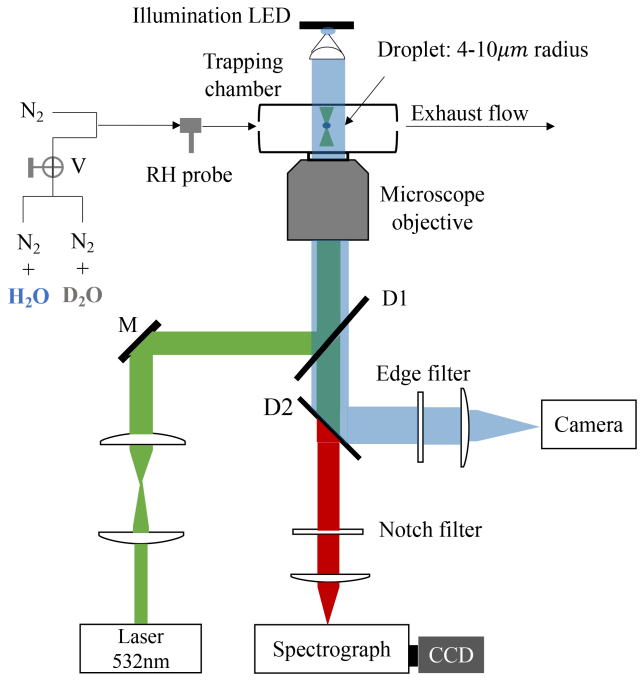

Figure 1. Schematic of the laser tweezer Raman spectroscopy system. A 532 nm laser beam was used to trap the aerosol droplet and excite its Raman signal. The droplet was imaged using a 470 nm illumination LED and a high-frame-rate camera. The Raman spectra of the trapped droplets were recorded using a spectrograph and a CCD. The RH in the aerosol trapping chamber was regulated by a flow of mixing N_2 / $N_2 + H_2O$ or N_2 / $N_2 + D_2O$. V is three-way valves. M is a mirror. D1 and D2 are dichroic mirrors.

trapping and a Raman-exciting light. The backscattering Raman light was conducted into a spectrograph (SpectaPro 2300i, Acton) equipped with a liquid-nitrogen-cooled CCD (Spec-10, Princeton Instruments) working at a temperature of −120 °C. The spectrograph grating used herein was 1200 grooves mm^{-1}, and the spectrometer resolution was $\sim 4\,cm^{-1}$.

Bulk solutions with desired chemical compositions were used to generate the aerosol droplets through a medical nebulizer (Mint PN100). In a tailored aerosol trapping chamber (Fig. S1), individual droplets (4–10 µm) from an incoming droplet train were trapped and levitated by the laser tweezers. More details of the LTRS system can be found in our previous works (Tong et al., 2022a, b, c). For D_2O with solute aerosols, a D_2O bubbler was first used to provide moisture in the trapping chamber; after the droplet equilibrated with the surrounding water vapor, the flow path was turned into a H_2O bubbler by three-way valves to observe the substitution of H_2O for D_2O within the droplet. For H_2O with solute aerosols, the moisture was first provided by the H_2O bubbler and then by the D_2O bubbler, and the substitution process of D_2O for H_2O was studied. The volume of the aerosol chamber was $< 24.7\,cm^3$ (Fig. S1). The gas-washing bottle used as a bubbler herein had a volume of 100 mL and contained 30 mL of D_2O. The total flux of dry and wet N_2 used herein was 100 sccm. Thus, at an RH of 60 %, the maximum time required for the chamber vapor to switch between H_2O and D_2O was 1.58 min, which can be identified as the response time of the chamber (formally τ_{cell}).

2.2 Detection of phase separation

The phase separation in substrate-deposited aerosols can be directly observed through bright-field imaging, transmission electron microscopy, or transmission X-ray microscopy (Pöhlker et al., 2012; You et al., 2012; Lee et al., 2020; Ma et al., 2021). However, for levitated droplets, the defocusing of the trapped droplets blurs the direct imaging. Instead, previous studies have shown that the time-resolved Raman spectra of the trapped droplets can be used to efficiently detect phase separation (Tong et al., 2022c; Gorkowski et al., 2016, 2018, 2020; Sullivan et al., 2020).

The trapped droplet works as an enhancing cavity and will overlap stimulated sharp peaks at wavelengths commensurate with whispering gallery modes (WGMs) on the spontaneous Raman spectra. The Raman spectra of aerosols with three different morphology archetypes are shown in Fig. S2. (i) The spectra containing high-quality WGMs indicate the isotropy within the particle and yield a homogenous morphology. (ii) The spectra containing weak but noticeable WGMs indicate the symmetry of the particle remains and yield a core–shell morphology. The shell thickness has appreciable influences on the aerosol spectrum. The weak WGMs may be caused by bad sphericity of the droplet, such as non-uniform shell thickness. A droplet with good spherical symmetry and deep WGM penetration induces well-resolved WGM peaks, while a droplet with a nonstatic core leads to non-uniform shell thickness and induces unstable WGMs. (iii) The spectra without any WGMs indicate the destruction of both isotropy and symmetry in the particle and yield a partly engulfed morphology. Alternatively, Stewart et al. (2015) put forward another two signatures to detect phase separation in aerosol. One is that if the droplet radius and refractive index calculated by the Mie scattering model present an abrupt change that is not realistic, the phase separation may have occurred. The other is that if we fit the Raman spectra with the Mie scattering model for a homogenous droplet and the fitting errors between the measured and simulated WGM peaks increase by orders of magnitude, the droplet can be determined as inhomogeneous. Herein, we deploy the signatures of WGMs and fitting errors to detect the phase separation. The homogenous Mie scattering fitting model used in this work was developed by Preston and Reid (2015).

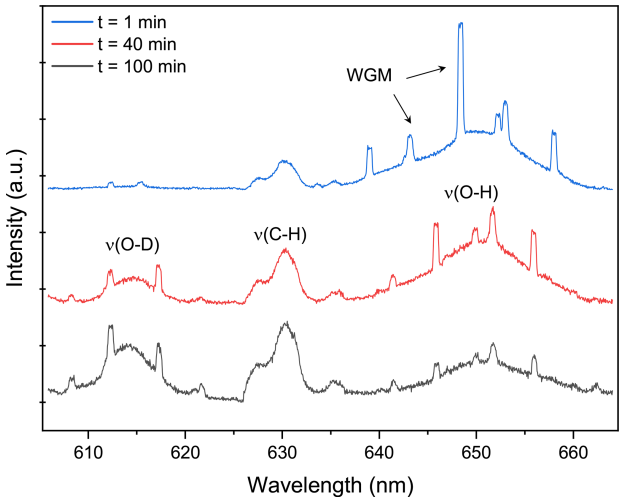

Figure 2. Raman spectrum snapshots of $H_2O + AS + DLT$ aerosol at different times during the water diffusion process. The set RH in the trapping chamber remained at 60 %. The blue, red, and black curves indicate the Raman spectrum extracted from Fig. 5a at 1, 40, and 100 min, which correspond to the initial, middle, and end stages of the water diffusion process, respectively. The WGMs and Raman feature bands are pointed out. When $t = 0$, it signifies the onset of switching H_2O moisture vapor to D_2O vapor.

3 Results

Here, we first detected the water diffusion in homogenous droplets to validate the performance of the isotope trace method. Then, the water diffusions in $H_2O + AS + OA$, $H_2O + AS + DLT$, and $H_2O + AS + HEX$ droplets were studied. The diffusion differences in these aerosols with different morphologies are discussed. Moreover, we added sulfuric acid to $H_2O + AS + DLT$ droplets and also discuss the influence of protons on water diffusion in aerosols.

3.1 Raman spectrum snapshots during water diffusion

Although H_2O and D_2O have nearly identical physical properties, O–D and O–H have different energy levels, which are therefore characterized with disparate Raman shifts (see the spectra of bulk H_2O and D_2O solutions in Fig. S3). Thus, the rise and fall of O–D / O–H peaks in Raman spectra can be used to trace water diffusion.

Figure 2 presents the representative stills of the Raman spectra of the $H_2O + AS + DLT$ droplet at different water diffusion progressions. The Raman peak assignment of representative atmospheric species has already been summarized in previous review papers (Liang et al., 2022; Estefany et al., 2023). The band range of 640–660 nm corresponded to the bending and stretching modes of O–H of water, the band in the range of 605–625 nm corresponded to the modes of O–D, and the range of 627–635 nm corresponded to the bending mode of C–H in organics (DLT here). It can be seen that at the early stage ($t = 1$ min) of water diffusion, the ν(O–H) was vastly predominant and the ν(O–D) was quite trivial. As water diffusion progresses ($t = 40$ min), the intensity of the ν(O–D) mode rose, while the intensity of the ν(O–H) mode fell. It indicated that with the surrounding moisture vapor being switched from H_2O to D_2O, the H_2O molecules within the droplet were being replaced by D_2O molecules, albeit under a constant-RH condition. For $t = 100$ min, ν(O–D) became predominant compared with ν(O–H), indicating that the droplet had changed from a H_2O droplet to a D_2O-dominating droplet. Compared with Fig. S3, it can be seen that both ν(O–H) and ν(O–D) modes in suspended aerosols were weaker than those in corresponding bulk solutions, which means the total water content in aerosols was far lower than that in their mother solutions. It underscores the advantage of this contactless single technique that without the surface perturbations, the component concentration in the aerosol can exceed its solubility limit.

Under a constant-RH condition, the total amount of water (D_2O plus H_2O) in the aerosol can be assumed to remain constant. Thus, the time-resolved fractional concentration of D_2O (denoted by ϕ_{OD}) can be calculated from the ν(O–H) and ν(O–D) modes at each spectral time:

$$\phi_{OD} = \frac{A_{OD}}{A_{OD} + \frac{1}{\sqrt{2}} A_{OH}}, \quad (1)$$

where A_{OD} and A_{OH} are the integrated intensities of the ν(O–D) and ν(O–H) modes, respectively. The factor of $1/\sqrt{2}$ before A_{OH} is to compensate for the difference in reduced mass between hydrogen and deuterium (Price et al., 2014; Nadler et al., 2019). Therefore, temporal variations in ϕ_{OD} retrieved from the aerosol Raman spectra can be used to quantify the water diffusion process. A caveat is that Fig. S4 shows the calculated ϕ_{OD} after effacing WGMs in the spectra, indicating that the contribution of WGMs to the peak areas is inconsequential. The O–H and O–D bands were quite broad, while the WGM peaks were somewhat narrow (Fig. 2). The fractional concentration of D_2O was retrieved from the Raman band area rather than the peak intensity; thus the interference of WGMs with ϕ_{OD} was trivial. The presented ϕ_{OD} was hereafter calculated by ignoring the WGM influences.

3.2 Water diffusion in homogenous aerosols

The water diffusion of a single $D_2O + CA$ aerosol exposed to H_2O moisture vapor is shown in Fig. 3. The droplet was first trapped and equilibrated in D_2O vapor. At $t = 0$, the manifold gas valves were rotated to switch from D_2O to H_2O. In Fig. 3a, it can be seen that, over time, the intensity of ν(O–D) deteriorated rapidly and that of ν(O–H) increased. Meanwhile, the intensity of ν(C–H) remained stable, indicating that the component concentration in the aerosol was roughly constant throughout the experiment. The existing WGMs in each spectrum mean that the droplet was spherically symmetric.

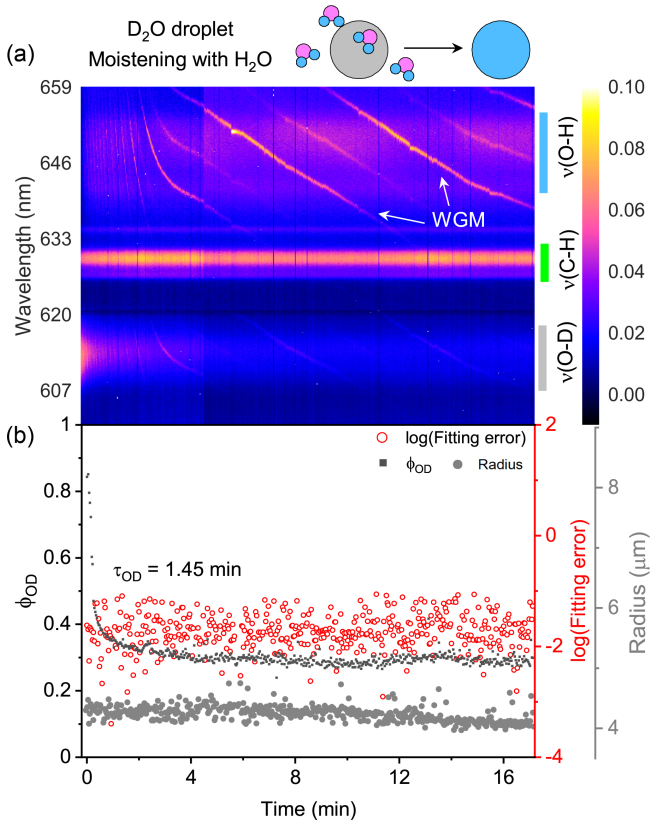

Figure 3. Water diffusion in a single homogenous $D_2O + CA$ aerosol at RH = 60 %. **(a)** The time-resolved cavity-enhanced Raman spectra of the droplet. The abscissa is the time, and the ordinate indicates the wavelength. The spectral intensity at each wavelength and time is illustrated with color. The WGMs are pointed out with white arrows. The top diagram depicts the water diffusion process, where light gray represents the D_2O phase, and blue represents the H_2O phase. The modes of ν(O–H), ν(C–H), and ν(O–D) are pointed out with different color bars on the right. **(b)** Black, the temporal variation in the fractional concentration of D_2O within the droplet; red, the fitting errors of the WGMs based on the homogenous Mie scattering model; gray, the fitted aerosol radius. τ_{OD} is the e-folding time of the ϕ_{OD} curve. When $t = 0$, it signifies the onset of switching from D_2O moisture vapor to H_2O vapor. The experiment was conducted at room temperature.

Of note, the WGMs shown in Fig. 3a (0–2 min) changed rapidly. It may have been induced by the change in the true RH experienced by the droplet. While the moisture was switched from D_2O to H_2O, the H_2O needed $\sim$ 1.6 min (τ_{cell}) to fill the chamber. However, during this period, dry nitrogen entered the chamber sustainedly, while H_2O molecules delayed in the bubbler bottle and gas tubes. The true RH experienced by the droplet may hence decrease, inducing the WGM shift. Furthermore, some spontaneous surface fluctuations, e.g., thermally induced capillary waves, existed in the optically trapped droplet (Endo et al., 2018; Pigot and Hibara, 2012; Chung et al., 2017). Surface fluctuations disturbed the standing wave at the interface between droplet and air, which may also contribute to the unstable spectral WGMs.

The temporal variation in ϕ_{OD} in Fig. 3b shows the substitution of H_2O for D_2O. The calculated e-folding time of the ϕ_{OD} curve (formally τ_{OD}) was 1.45 min, indicating that the homogenous aerosol can promptly respond to the variation in the surrounding atmosphere. However, $\tau_{OD} < \tau_{cell}$ implies that H_2O had started to diffuse into the droplet before the gas exchange from D_2O to H_2O was completed. Hence, water diffusion in a homogenous CA droplet may be even faster than Fig. 3 shows. Figure 3b shows that the fitting errors of the measured WGMs calculated by the homogenous Mie scattering model were of the order of 10^{-2}, which is quite small (compared with Fig. 7). It means that the droplet was well mixed and isotropic. CA is a water-soluble organic compound; thus the suspended $D_2O + CA$ aerosol was homogenous and had a spherical shape. It was validated by both the WGMs in the spectra and the fitting errors. The water diffusion of the CA droplet at lower RH (20 %) is shown in Fig. S6. The retrieved τ_{OD} was 13.67 min, which was longer than that at RH = 60 %, indicating that water diffusion was retarded under very-low-RH conditions. This result agreed well with previous works (Table S1), validating the performance of our system.

3.3 Water diffusion in partly engulfed aerosols

The oleic acid is a preferential proxy of water-insoluble organics in ambient aerosols. Herein, the $H_2O + AS + OA$ droplet was generated by nebulizing a mixed solution containing AS, OA, and water. The volume ratio of the OA + AS mother solution was 4/1 (aqueous AS / OA). The mixture was fully shaken to form an aqueous OA emulsion before nebulization. Thus, a number of OA inclusions would be contained in the nascent droplet. The OA content in the droplet herein was random. If the droplet spectra could not support a partly engulfed morphology, the droplet was released until one spectra-confirmed partly engulfed droplet was captured. The droplet was trapped and equilibrated in H_2O vapor. Then the vapor was switched from H_2O to D_2O.

Figure 4 shows the water diffusion in a single $H_2O + AS + OA$ aerosol. Figure 4a shows no evident WGMs in the aerosol spectrum, indicating the destruction of both isotropy and symmetry in the particle. Thus, the droplet should have a partly engulfed morphology after reaching a thermodynamic equilibrium with the surrounding moisture, where a hydrophobic cap of OA encases an aqueous phase. Ishizaka et al. (2021) reported that the hydrophobic phase was not always at the bottom of the droplet; thus the herein observed spectral variation at $t = \sim$ 60 min may stem from the drift of the hydrophobic cap. The volume ratio of the aqueous phase and hydrophobic phase in the trapped droplet cannot be preset because of the stochastic mixing of OA emulsions and water during nebulizing. If an approximately spherical cavity occurs for the aqueous volume, the WGM

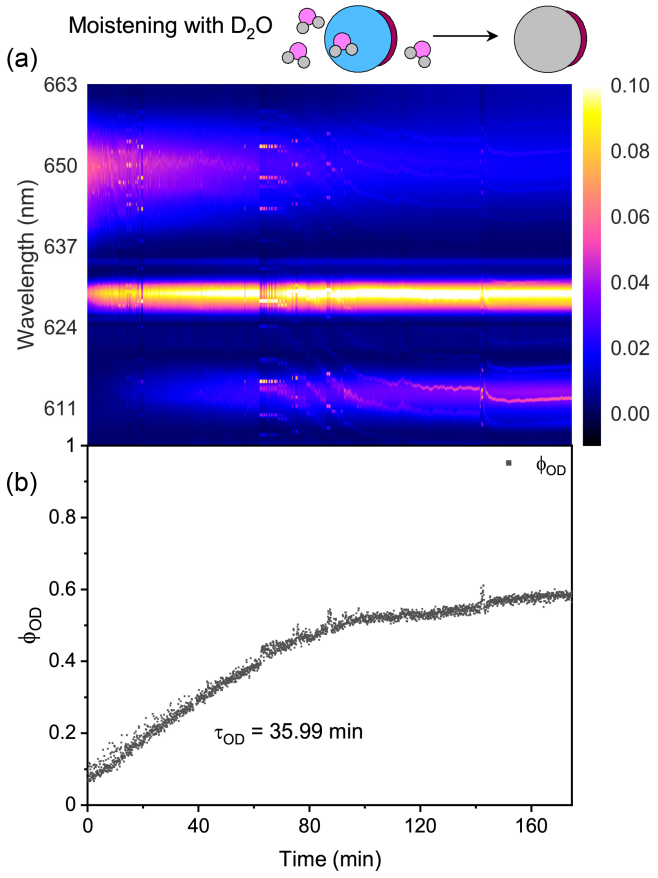

Figure 4. Water diffusion in a single phase-separated $H_2O + AS + OA$ aerosol at RH = 60 %. **(a)** The time-resolved Raman spectra of the droplet. The top diagram depicts the water diffusion process in the partly engulfed aerosol, where light gray represents the D_2O phase, blue represents the H_2O phase, and dark red represents the hydrophobic organic phase. **(b)** The temporal variation in the fractional concentration of D_2O within the droplet. When $t = 0$, it signifies the onset of the switch from H_2O moisture vapor to D_2O vapor. The experiment was conducted at room temperature.

fingerprint of the droplet may be of low quality and complexity. Moreover, the band of C–H here was stronger than that in Fig. 3a, which may result from the fact that the OA molecule has more C–H bonds than CA.

The ϕ_{OD} shown in Fig. 4b changed more slowly than that in Fig. 3b. The calculated τ_{OD} of the $H_2O + AS + OA$ aerosol was $\sim$ 35.99 min, which was 25 times longer than that of $D_2O + CA$. It means that an inhibition of gas–particle partitioning occurred in such a phase-separated droplet. The OA phase in the droplet had a considerably strong hydrophobicity, which may prevent the moisture from diffusing through the organic cap. The effective interface between the aqueous phase and the air reduced because of the phase separation, leading to a slower water diffusion compared with the homogenous aerosol.

3.4 Water diffusion in core–shell aerosols

The core–shell morphology is another prevailing phase-separated morphology of ambient aerosols. Here, we generated aerosol droplets from mother solutions containing $H_2O + AS + DLT$ and $H_2O + AS + HEX$ and induced phase separation in them by presetting the surrounding RH below their separation relative humidity (SRH; the RH level at which phase separation occurs). The droplets were trapped and equilibrated in H_2O vapor before switching the moisture vapor from H_2O to D_2O.

Figure 5 presents the diffusion of D_2O and H_2O in a single $H_2O + AS + DLT$ droplet during a 7 h observation at RH = 60 %. As shown in Fig. 5a, the log (fitting errors) throughout the observation was roughly higher than -1, which was 1 order higher than the homogenous aerosol errors, indicating that the droplet was not homogenous. Furthermore, the WGMs persisted in the whole observation; thus the droplet should be core–shell.

To provide detailed insights into the phase-separated structure, we used a core–shell Mie model developed by Vennes and Preston (2019) to calculate the core and shell radii of the droplet (see more details in Sect. S7). In Fig. 6, it can be seen that for the spectra shown in Fig. 5a (t = 0–110 min), the calculated particle radius was around 5 µm, and the fluctuation was quite trivial. Meanwhile, the calculated radius ratio (i.e., the ratio of the core radius to the whole particle radius) was around 0.8, which yielded a core radius of 4 µm and a shell thickness of 1 µm. The results validated that at RH = 60 %, the liquid–liquid phase separation occurred in the $H_2O + AS + DLT$ aerosol, and the separated morphology was core–shell.

For t = 0–160 min (denoted by Stage I), the droplet was moistened by D_2O vapor, and D_2O molecules started to diffuse into the droplet. The intensity of the O–H band in Fig. 5a decreased, while the intensity of the O–D band increased; this variation is crystal clear in Fig. 5b, where ϕ_{OD} grew and ϕ_{OH} fell over time. However, in this stage where D_2O diffused into the droplet, the ϕ_{OD} plateaued to a constant value of 0.55 after more than 150 min diffusion, indicating that the H_2O molecules in the initial droplet could not be replaced completely by the surrounding gas-phase D_2O molecules. The intensity of the O–H band could not diminish to zero in the exchange process. Similar results can also be seen in the partly engulfed aerosol and even in the homogenous aerosol, where the final values of ϕ_{OD} were 0.6 and 0.3, respectively. Previous works have reported such kinetic limitations of diffusion in ultra-viscous or amorphous-state aerosols: significant radial gradients in pH (Wei et al., 2018), solute concentrations (Zobrist et al., 2008), and reactant uptake (Virtanen et al., 2010; Davies and Wilson, 2015; Gaston and Thornton, 2016) solidly existed in ambient aerosols. A possible explanation is that certain molecule clusters composed of hydroxyls, electrolytes, and organics formed in the aerosols because of supersaturation, which protected a hand-

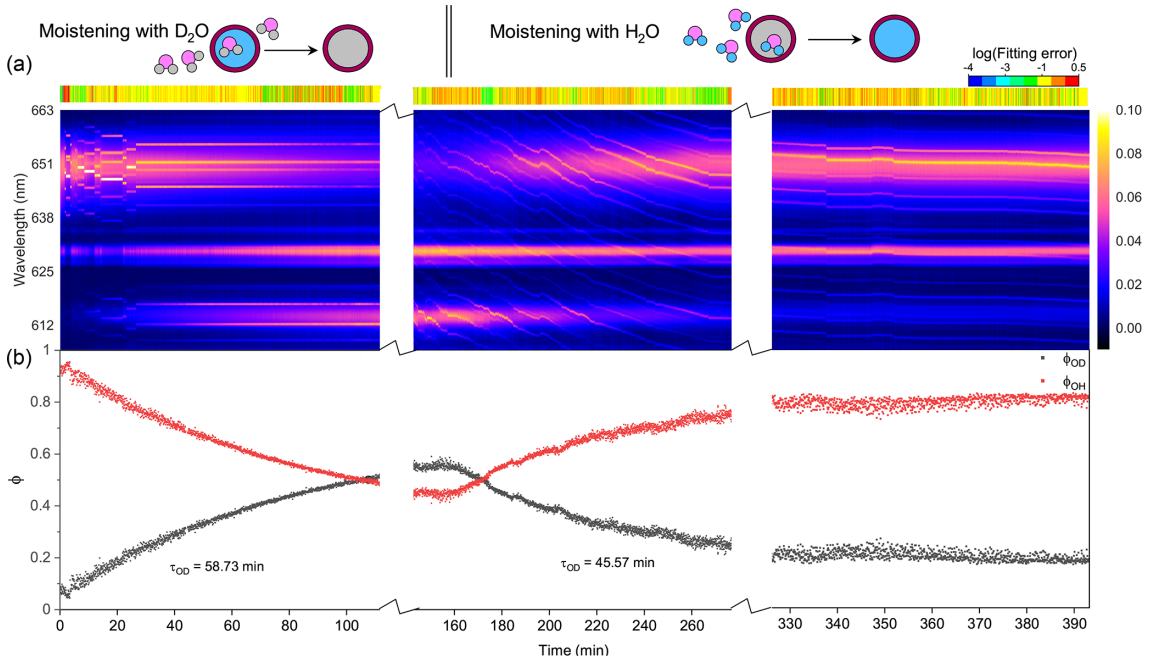

Figure 5. Water diffusion in a single phase-separated $H_2O + AS + DLT$ aerosol at RH = 60 %. **(a)** The time-resolved cavity-enhanced Raman spectra of the droplet. The top color bars indicate the log (fitting errors) of the WGMs based on the homogenous Mie scattering model. The running of the spectrograph needed a break to avoid overloading the shutter, which caused the hiatuses in the spectra. **(b)** Black, the temporal variation in the fractional concentration of D_2O within the droplet; red, the temporal variation in the fractional concentration of H_2O within the droplet; $\phi_{OH} = 1 - \phi_{OD}$. The droplet was first trapped and equilibrated in H_2O vapor. When $t = 0$, it signifies the onset of the switch from H_2O moisture vapor to D_2O vapor. At $t = 160$ min, the moisture vapor was switched back from D_2O to H_2O. The experiment was conducted at room temperature.

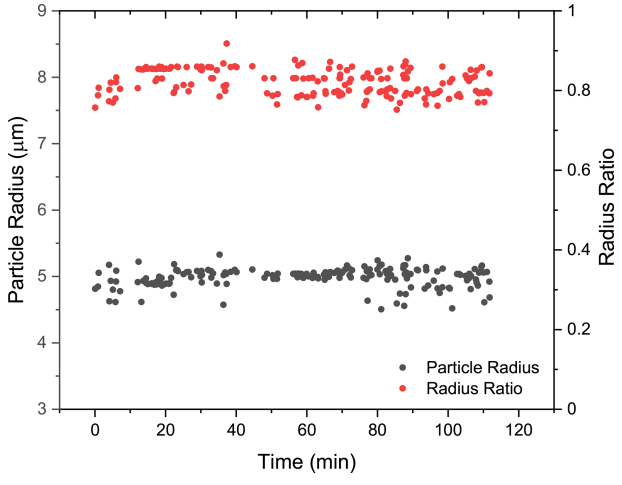

Figure 6. Radius of the phase-separated $H_2O + AS + DLT$ aerosol at RH = 60 %. Black, the aerosol radius; red, the ratio of the core radius to the whole particle radius. The results were obtained by fitting the spectra in Fig. 5a ($t = 0$–110 min) with a core–shell model developed by Vennes and Preston (2019) .

ful of H_2O molecules in the aerosols from being replaced by D_2O molecules. Moreover, as water diffusion progressed, the diffusion-driving forces attenuated because of the reducing deviation of vapor pressures between the gas and particle phase, which might both decrease the success of surface accommodation of gas molecules and make the solvation through the particle bulk more difficult, rendering an incomplete molecule substitution.

For $t > 160$ min (denoted by Stage II), the moisture vapor was switched back from D_2O to H_2O. In Fig. 5a, it can be seen that the Raman band of O–H rebounded and that of O–D declined over time. After molecules diffused for 4 h, ϕ_{OD} did not diminish to 0, and ϕ_{OH} did not return to 1, yielding a similar incomplete substitution. Noteworthily, in Fig. 5b, throughout Stages I and II, the maximum of ϕ_{OH} was 0.8, which was higher than that of ϕ_{OD}. This indicates that, at the later stage of diffusion, D_2O was harder to partition into the particle phase compared with H_2O. Considering the virtually identical chemistry of these two molecules, the difference in molecular mass may give rise to the different final diffusion extent. From another perspective, during the process of aerosol trapping, the generated aerosol train may condense some droplets on the walls of the chamber and tubes. The H_2O molecules within these droplets may then interfere with the subsequent water diffusion.

As shown in Fig. 5b, the τ_{OD} of Stages I and II was 58.7 and 45.6 min, respectively, which were both higher than that of partly engulfed aerosol and homogenous aerosol. The av-

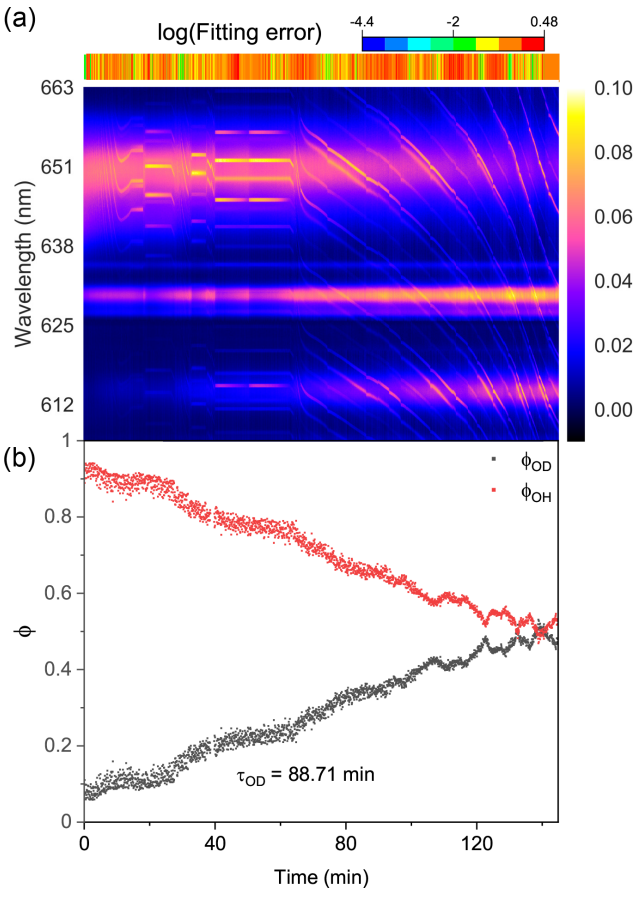

Figure 7. Water diffusion in a single phase-separated $H_2O + AS + HEX$ aerosol at RH = 60 %. **(a)** The time-resolved cavity-enhanced Raman spectra of the droplet. The top color bars indicate the log (fitting errors) of the WGMs based on the homogenous Mie scattering model. **(b)** The temporal variations in the fractional concentration of water molecules within the droplet. The droplet was first trapped and equilibrated in H_2O vapor. When $t = 0$, it signifies the onset of the switch from H_2O moisture vapor to D_2O vapor. The experiment was conducted at room temperature.

erage τ_{OD} was 52.2 min, which was 1.5 times that of the partly engulfed aerosol and 36 times that of the homogenous aerosol, implying a more profound diffusion inhibition in core–shell aerosols. With the organic shell totally encasing the aqueous core, the moisture molecules had to penetrate through the shell during diffusion, which vastly retarded the molecule exchange.

We then observed the water diffusion in a single $H_2O + AS + HEX$ aerosol. Figure 7 shows the recorded Raman spectra and variations in fractional concentrations. At $t = 0$, D_2O vapor started to moisten the H_2O droplet. The results of the log (fitting errors) and spectral WGMs indicated that the droplet was phase-separated with a core–shell morphology throughout the observation. With the droplet being exposed to the D_2O vapor, the Raman O–H band diminished and the O–D band rose. However, as shown in Fig. 7b, the calculated τ_{OD} was 88.7 min, implying a more severe diffusion inhibition compared with the $H_2O + AS + DLT$ aerosol. Ma et al. (2021) reported that the structure of the phase-separated $AS + HEX$ droplet was considerably complex at RH = 60 %, where a HEX-rich shell, an AS-rich core, and more concentrated AS inclusions in the core coexisted. The force between AS and water molecules, particularly in the concentrated AS inclusions, was much stronger than that between HEX and water. Bound water may form in this circumstance. The substitution of D_2O for H_2O needed to overcome the bound water force, which might be quite difficult because the solute concentration in the AS inclusions was far beyond its solubility limit. This may contribute to the slow water diffusion in the $AS + HEX$ droplet. Moreover, Richards et al. (2020) reported that supramolecular ion–organic interactions may exist when aerosols contain organics (specifically those containing vicinal hydroxyl groups) and inorganic divalent ions, which produces internal cross-linking molecular networks. Such ion–organic networks might have formed in the shell of the $H_2O + AS + HEX$ aerosol and thus blocked the passage of water molecules.

Protons are considered to have appreciable impacts on the phase separation in ambient aerosols (Tong et al., 2022c; Dallemagne et al., 2016; Losey et al., 2016). Here, we added sulfuric acid to $H_2O + AS + DLT$ droplets and observed the water diffusion process in the resultant acidified aerosols. The pH of the mother solution to generate aerosols was preset to 1.17. Figure 8 shows the recorded Raman spectra and variations in the fractional concentrations of a single acidified $H_2O + AS + DLT$ droplet. The results of the log (fitting errors) and spectral WGMs indicated that the droplet was homogenous. After being moistened by D_2O vapor at $t = 0$, the Raman O–H band faded and the O–D band increased. The τ_{OD} shown in Fig. 8b was 17.4 min, which was less than the value of the two types of phase-separated aerosols. It shows that the surplus protons improved water diffusion in $H_2O + AS + DLT$ aerosols, which indicated that the added sulfuric acid may impede the occurrence of phase separation. The aerosol pH was reported to have significant impacts on liquid–liquid phase separation. However, the impacts were different and related to the organic component. Previous works have found that the SRH of some organic acids (e.g., 3-methylglutaric acid) increased as the aerosol pH decreased (Losey et al., 2016), while the SRH of other organics (e.g., polyols) decreased as the pH decreased (Losey et al., 2018). From a fundamental physical chemistry perspective, the fluctuations in the local solute concentration will lead to thermodynamic instability in the droplet structure and subsequently induce phase separation. Herein, the added sulfuric acid increased droplet viscosity and reduced its liquidity, which may limit concentration fluctuations and promote homogeneity.

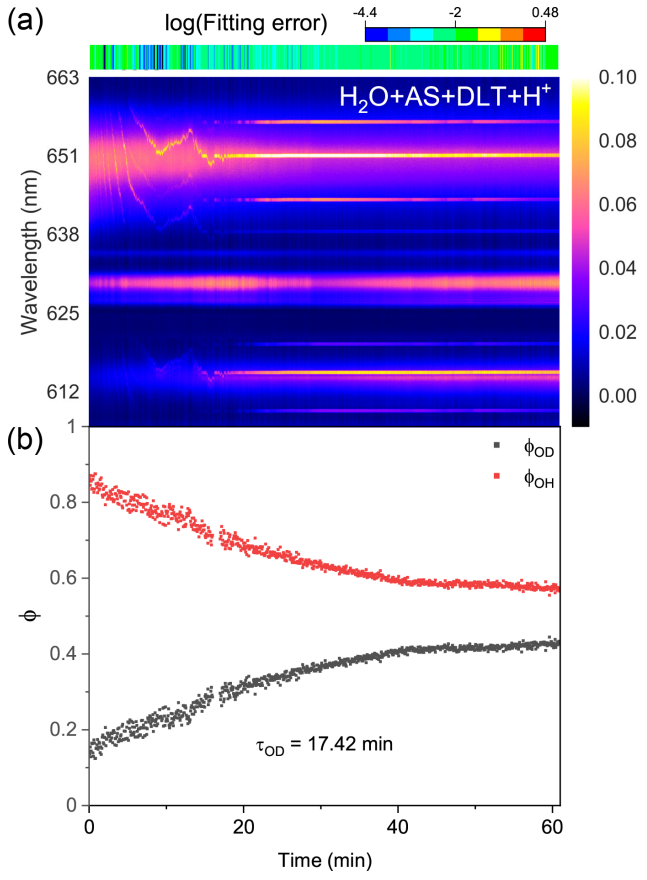

Figure 8. Water diffusion in single acidified $H_2O + AS + DLT$ aerosol at RH = 60 %. **(a)** The time-resolved cavity-enhanced Raman spectra of the droplet. The top color bars indicate the log (fitting errors) of the WGMs based on the homogenous Mie scattering model. **(b)** The temporal variations in the fractional concentration of water molecules within the droplet. The droplet was first trapped and equilibrated in H_2O vapor. When $t = 0$, it signifies the onset of the switch from H_2O moisture vapor to D_2O vapor. The experiment was conducted at room temperature.

4 Discussion

The isotope exchange during the water diffusion process in single aerosols can be well elucidated by the solution to Fick's second law for a sphere (Price et al., 2014; Moridnejad and Preston, 2016; Nadler et al., 2019) :

$$\phi_{OD} = 1 - \left(\frac{6}{\pi^2}\right)\sum_{n=1}^{\infty}\frac{1}{n^2}\exp\left(-\frac{n^2\pi^2 D_w t}{a^2}\right), \quad (2)$$

where a is the particle radius and D_w is the diffusion coefficient of water. A prerequisite of applying the Fickian diffusion model is that the particle achieves a homogenous mixture after sufficient equilibration time, which is however not available for the aerosols studied here. Thus, a modified Fickian diffusion model (Eq. 3) is used to analyze the observed incomplete isotope exchange, where a correction factor χ is introduced to reveal the diffusion limitation and indicate the diffusing extent,

$$\phi_{OD} = \chi\left[1 - \left(\frac{6}{\pi^2}\right)\sum_{n=1}^{\infty}\frac{1}{n^2}\exp\left(-\frac{n^2\pi^2 D_w t}{a^2}\right)\right]. \quad (3)$$

The radii of the aerosols can be determined by bright-field imaging and the core–shell Mie model. Then, D_w can be expediently derived by using a three-term expansion of the modified Fickian diffusion model to fit the temporal variations of ϕ_{OD} retrieved from the Raman spectra. An application of the diffusion model to the isotope exchange data is shown in Fig. S5. The water diffusion coefficients of the aforementioned aerosols are summarized in Table 1. The comparison between the measured water diffusion coefficients in this work and those of literature works can be seen in Sect. S6. The measured D_w of phase-separated droplets was considerably lower than the values of homogenous droplets studied in literature works, indicating the occurrence of the water diffusion limitations.

The isotope exchange method has some experimental limitations. For example, the spectral acquisition costs time; after switching H_2O to D_2O, it also takes time to fully replace the composition of the atmosphere in the trapping chamber. Due to these inevitable time limitations, the isotope exchange method does not adapt to quantifying the rapid diffusion circumstance, leading to an upper limit of diffusion coefficient measuring of $\sim 10^{-13}$ m^2 s^{-1} (Davies and Wilson, 2016; Nadler et al., 2019). The water diffusion in the $D_2O + CA$ droplet was quite fast; hence the onset of water diffusion could not be exactly determined. As shown in Sect. 3.2, the observed τ_{OD} did not closely mirror the rate of water diffusion. Thus, the D_w of the $D_2O + CA$ aerosol was not calculated in Table 1. The $H_2O + AS + OA$ aerosol was treated as an approximate sphere. The measured D_w decreased in the order of homogenous, partly engulfed, and core–shell aerosols, which was in line with the diffusion rate presented in Sect. 3.

The parameter of the first exponential term in Eq. (2) (i.e., $\pi^2 D_w/a^2$) indicates the rate of diffusion for a homogenous aerosol, the reciprocal of which means the equilibrium mixing time (denoted by τ_{mixing}) of volatile molecules within the homogenous aerosol. According to the modified Fickian diffusion model, the fitted τ_{mixing} of $H_2O + AS + DLT$ was 182 min (see Fig. S5). However, in Fig. 5b, it can be seen that when $t = 130$ min, the ϕ_{OD} leveled off, which means the diffusion of D_2O had reached a balance. The observed equilibrium diffusion time was less than the calculated τ_{mixing}. It implies that the water molecules within these aerosols did not diffuse to an isotropically stable state; thus concentration gradients existed in the aerosols. It revalidated the deductions from the final value of ϕ_{OD}. If considering the correction factor χ, the $\chi\tau_{mixing}$ of $H_2O + AS + DLT$ was 132 min, which agreed well with the experimental observation. It means the

Table 1. Water diffusion coefficients of aerosols with various morphologies at RH = 60 %.

Aerosol	Morphology	τ_{OD} (min)	χ	D_w ($\times 10^{-16}$ m^2 s^{-1})
$D_2O + CA$	homogenous	1.45	n/a	n/a
$H_2O + AS + OA$	partly engulfed	35.99	0.77 ± 0.013	13.18 ± 0.63
$H_2O + AS + DLT$ (Stage I)	core–shell	58.73	0.73 ± 0.016	5.36 ± 0.33
$H_2O + AS + HEX$	core–shell	88.71	0.65 ± 0.029	2.25 ± 0.15
$H_2O + AS + DLT + H^+$	homogenous	17.42	0.49 ± 0.004	39.96 ± 0.11

n/a: not applicable.

modified Fickian diffusion model works well to simulate the water diffusion presented here.

The χ of $H_2O + AS + DLT$ was 0.7, which means that 70 % of the total H_2O molecules in the droplet were substituted by D_2O molecules. The χ of $H_2O + AS + HEX$ was 0.65, indicating that its more complex phase-separated structure led to a lower diffusion extent of D_2O than $H_2O + AS + DLT$. Contrastingly, the χ of the $H_2O + AS + OA$ aerosol was 0.77, which indicated that the partly uncovered gas–particle interface allowed for a higher diffusion extent of D_2O than the core–shell aerosols. Of note, the χ of the $H_2O + AS + DLT + H^+$ aerosol was 0.5, which was lower than the partly engulfed and core–shell aerosols. A fair number of studies have reported the existence of hydrated proton clusters with diverse structures in acid solutions (Headrick et al., 2005; Biswas et al., 2017; Knight and Voth, 2012; Agmon et al., 2016). Therefore, the hydrated proton clusters in the acidified $H_2O + AS + DLT$ aerosol may preclude the substitution of D_2O for H_2O and give rise to a low diffusion extent. Moreover, the existence of bound water may limit water molecule evaporation and reduce the equilibrium water vapor pressure at the surface of acidified homogenous droplets (solute effect). While the surrounding moisture was switched from H_2O to D_2O, H_2O molecules within the droplet began to evaporate into the gas to keep its vapor pressure equal to the equilibrium pressure. Lower equilibrium vapor pressure means a weaker driven force of diffusion; thus the water molecule substitution in the droplet with low pH was not as fast as in the neutral homogenous droplet. Such a diffusion limitation may provide a possible explanation for the long lifetime of certain ambient aerosols of which the unreacted core species were protected from potential surface-sensitive phenomena such as cloud condensation nucleation and ice nucleation activities (Zhang et al., 2019; Adachi and Buseck, 2008; Kanji et al., 2019; Yu et al., 2019).

5 Conclusions

In this work, we characterized the water diffusion process in single suspended phase-separated aerosols via a self-constructed laser tweezer Raman spectroscopy system. The recorded Raman spectra of the aerosols were used to detect their morphology and observe the exchange of D_2O / H_2O molecules. The results of the core–shell aerosols show that water molecules can pass through the organic shell and diffuse into the particle bulk, and the diffusion rate depended on the type of the organic compound. The partly engulfed and homogenous aerosols had higher diffusion rates compared with core–shell aerosols. The results of the acidified $H_2O + AS + DLT$ aerosol show that protons can improve water diffusion in the aerosol, indicating that acid inhibited phase separation. Moreover, incomplete diffusion was observed in all three types of aerosols with different morphologies. By measuring the water diffusion coefficients and diffusion extents with a modified Fickian diffusion model, we found that 65 %–75 % of the total H_2O molecules in the phase-separated aerosols were substituted by D_2O molecules, which implies that certain molecule clusters formed in the aerosols.

More work on the reactive uptake of gas molecules into phase-separated aerosols should be done in the future. Additionally, considering that the sizes of the droplets studied here were 4–10 µm, it is imperative to develop techniques for detecting water diffusion in smaller phase-separated droplets in the future.

Code and data availability. The datasets generated during this study are available at Peking University's Open Research Data Platform: https://doi.org/10.18170/DVN/LJMWYV (Tong et al., 2024).

Supplement. The supplement related to this article is available online at: https://doi.org/10.5194/acp-24-2937-2024-supplement.

Author contributions. YKT proposed the idea of the project, performed the experiments, conducted the data analysis, and led in writing the paper. AY contributed to funding the research, constructed the optical tweezer system, provided the instructions for the experiment, and revised the paper. ZW and MH discussed the methodology and revised the paper.

Competing interests. The contact author has declared that none of the authors has any competing interests.

Acknowledgements. Yu-Kai Tong gratefully acknowledges Bo Zhou and Rui Sun for meaningful discussions on data visualization.

Financial support. This research has been supported by the National Natural Science Foundation of China (grant nos. U19A2007, 32150026, and 92043302).

Review statement. This paper was edited by Thomas Berkemeier and reviewed by two anonymous referees.

References

Adachi, K. and Buseck, P. R.: Internally mixed soot, sulfates, and organic matter in aerosol particles from Mexico City, Atmos. Chem. Phys., 8, 6469–6481, https://doi.org/10.5194/acp-8-6469-2008, 2008.

Agmon, N., Bakker, H. J., Campen, R. K., Henchman, R. H., Pohl, P., Roke, S., Thämer, M., and Hassanali, A.: Protons and Hydroxide Ions in Aqueous Systems, Chem. Rev., 116, 7642–7672, https://doi.org/10.1021/acs.chemrev.5b00736, 2016.

Aristov, Y. I., Glaznev, I. S., Freni, A., and Restuccia, G.: Kinetics of water sorption on SWS-1L (calcium chloride confined to mesoporous silica gel): Influence of grain size and temperature, Chem. Eng. Sci., 61, 1453–1458, https://doi.org/10.1016/j.ces.2005.08.033, 2006.

Bishop, A. I., Nieminen, T. A., Heckenberg, N. R., and Rubinsztein-Dunlop, H.: Optical Microrheology Using Rotating Laser-Trapped Particles, Phys. Rev. Lett., 92, 198104, https://doi.org/10.1103/PhysRevLett.92.198104, 2004.

Biswas, R., Carpenter, W., Fournier, J. A., Voth, G. A., and Tokmakoff, A.: IR spectral assignments for the hydrated excess proton in liquid water, J. Chem. Phys., 146, 154507, https://doi.org/10.1063/1.4980121, 2017.

Bones, D. L., Reid, J. P., Lienhard, D. M., and Krieger, U. K.: Comparing the mechanism of water condensation and evaporation in glassy aerosol, P. Natl. Acad. Sci. USA, 109, 11613–11618, https://doi.org/10.1073/pnas.1200691109, 2012.

Booth, A. M., Murphy, B., Riipinen, I., Percival, C. J., and Topping, D. O.: Connecting Bulk Viscosity Measurements to Kinetic Limitations on Attaining Equilibrium for a Model Aerosol Composition, Environ. Sci. Technol., 48, 9298–9305, https://doi.org/10.1021/es501705c, 2014.

Cai, C., Tan, S., Chen, H., Ma, J., Wang, Y., Reid, J. P., and Zhang, Y.: Slow water transport in MgSO4 aerosol droplets at gel-forming relative humidities, Phys. Chem. Chem. Phys., 17, 29753–29763, https://doi.org/10.1039/C5CP05181A, 2015.

Cao, W., Knudsen, K., Fredenslund, A., and Rasmussen, P.: Group-contribution viscosity predictions of liquid mixtures using UNIFAC-VLE parameters, Ind. Eng. Chem. Res., 32, 2088–2092, https://doi.org/10.1021/ie00021a034, 1993.

Chan, M. N., Lee, A. K. Y., and Chan, C. K.: Responses of Ammonium Sulfate Particles Coated with Glutaric Acid to Cyclic Changes in Relative Humidity: Hygroscopicity and Raman Characterization, Environ. Sci. Technol., 40, 6983–6989, https://doi.org/10.1021/es060928c, 2006.

Chung, M., Pigot, C., Volz, S., and Hibara, A.: Optical Surface Tension Measurement of Two-Dimensionally Confined Liquid Surfaces, Anal. Chem., 89, 8092–8096, https://doi.org/10.1021/acs.analchem.7b01611, 2017.

Dallemagne, M. A., Huang, X. Y., and Eddingsaas, N. C.: Variation in pH of Model Secondary Organic Aerosol during Liquid–Liquid Phase Separation, J. Phys. Chem. A, 120, 2868–2876, https://doi.org/10.1021/acs.jpca.6b00275, 2016.

Davies, J. F. and Wilson, K. R.: Nanoscale interfacial gradients formed by the reactive uptake of OH radicals onto viscous aerosol surfaces, Chem. Sci., 6, 7020–7027, https://doi.org/10.1039/C5SC02326B, 2015.

Davies, J. F. and Wilson, K. R.: Raman Spectroscopy of Isotopic Water Diffusion in Ultraviscous, Glassy, and Gel States in Aerosol by Use of Optical Tweezers, Anal. Chem., 88, 2361–2366, https://doi.org/10.1021/acs.analchem.5b04315, 2016.

Davies, J. F., Miles, R. E. H., Haddrell, A. E., and Reid, J. P.: Influence of organic films on the evaporation and condensation of water in aerosol, P. Natl. Acad. Sci. USA, 110, 8807–8812, https://doi.org/10.1073/pnas.1305277110, 2013.

Drozd, G. T., Woo, J. L., and McNeill, V. F.: Self-limited uptake of α-pinene oxide to acidic aerosol: the effects of liquid–liquid phase separation and implications for the formation of secondary organic aerosol and organosulfates from epoxides, Atmos. Chem. Phys., 13, 8255–8263, https://doi.org/10.5194/acp-13-8255-2013, 2013.

Endo, T., Ishikawa, K., Fukuyama, M., Uraoka, M., Ishizaka, S., and Hibara, A.: Spherical Spontaneous Capillary-Wave Resonance on Optically Trapped Aerosol Droplet, J. Phys. Chem. C, 122, 20684–20690, https://doi.org/10.1021/acs.jpcc.8b03784, 2018.

Estefany, C., Sun, Z., Hong, Z., and Du, J.: Raman spectroscopy for profiling physical and chemical properties of atmospheric aerosol particles: A review, Ecotoxicol. Environ. Safety, 249, 114405, https://doi.org/10.1016/j.ecoenv.2022.114405, 2023.

Fitzgerald, C., Hosny, N. A., Tong, H., Seville, P. C., Gallimore, P. J., Davidson, N. M., Athanasiadis, A., Botchway, S. W., Ward, A. D., Kalberer, M., Kuimova, M. K., and Pope, F. D.: Fluorescence lifetime imaging of optically levitated aerosol: a technique to quantitatively map the viscosity of suspended aerosol particles, Phys. Chem. Chem. Phys., 18, 21710–21719, https://doi.org/10.1039/C6CP03674K, 2016.

Fowler, K., Connolly, P., and Topping, D.: Modelling the effect of condensed-phase diffusion on the homogeneous nucleation of ice in ultra-viscous particles, Atmos. Chem. Phys., 20, 683–698, https://doi.org/10.5194/acp-20-683-2020, 2020.

Freedman, M. A.: Phase separation in organic aerosol, Chem. Soc. Rev., 46, 7694–7705, https://doi.org/10.1039/C6CS00783J, 2017.

Freedman, M. A.: Liquid–Liquid Phase Separation in Supermicrometer and Submicrometer Aerosol Particles, Account. Chem. Res., 53, 1102–1110, https://doi.org/10.1021/acs.accounts.0c00093, 2020.

Gaston, C. J. and Thornton, J. A.: Reacto-Diffusive Length of N_2O_5 in Aqueous Sulfate- and Chloride-Containing Aerosol Particles, J. Phys. Chem. A, 120, 1039–1045, https://doi.org/10.1021/acs.jpca.5b11914, 2016.

Gorkowski, K., Beydoun, H., Aboff, M., Walker, J. S., Reid, J. P., and Sullivan, R. C.: Advanced aerosol optical tweezers chamber design to facilitate phase-separation and equilibration timescale experiments on complex droplets, Aerosol Sci. Tech., 50, 1327–1341, https://doi.org/10.1080/02786826.2016.1224317, 2016.

Gorkowski, K., Donahue, N. M., and Sullivan, R. C.: Emerging investigator series: determination of biphasic core–shell droplet properties using aerosol optical tweezers, Environ. Sci. Process. Impacts, 20, 1512–1523, https://doi.org/10.1039/C8EM00166A, 2018.

Gorkowski, K., Donahue, N. M., and Sullivan, R. C.: Aerosol Optical Tweezers Constrain the Morphology Evolution of Liquid-Liquid Phase-Separated Atmospheric Particles, Chem, 6, 204–220, https://doi.org/10.1016/j.chempr.2019.10.018, 2020.

Hallquist, M., Wenger, J. C., Baltensperger, U., Rudich, Y., Simpson, D., Claeys, M., Dommen, J., Donahue, N. M., George, C., Goldstein, A. H., Hamilton, J. F., Herrmann, H., Hoffmann, T., Iinuma, Y., Jang, M., Jenkin, M. E., Jimenez, J. L., Kiendler-Scharr, A., Maenhaut, W., McFiggans, G., Mentel, Th. F., Monod, A., Prévôt, A. S. H., Seinfeld, J. H., Surratt, J. D., Szmigielski, R., and Wildt, J.: The formation, properties and impact of secondary organic aerosol: current and emerging issues, Atmos. Chem. Phys., 9, 5155–5236, https://doi.org/10.5194/acp-9-5155-2009, 2009.

Headrick, J. M., Diken, E. G., Walters, R. S., Hammer, N. I., Christie, R. A., Cui, J., Myshakin, E. M., Duncan, M. A., Johnson, M. A., and Jordan, K. D.: Spectral Signatures of Hydrated Proton Vibrations in Water Clusters, Science, 308, 1765–1769, https://doi.org/10.1126/science.1113094, 2005.

Ishizaka, S., Yamamoto, C., and Yamagishi, H.: Liquid–Liquid Phase Separation of Single Optically Levitated Water–Ionic Liquid Droplets in Air, The J. Phys. Chem. A, 125, 7716–7722, https://doi.org/10.1021/acs.jpca.1c06130, 2021.

Kanji, Z. A., Sullivan, R. C., Niemand, M., DeMott, P. J., Prenni, A. J., Chou, C., Saathoff, H., and Möhler, O.: Heterogeneous ice nucleation properties of natural desert dust particles coated with a surrogate of secondary organic aerosol, Atmos. Chem. Phys., 19, 5091–5110, https://doi.org/10.5194/acp-19-5091-2019, 2019.

Knight, C. and Voth, G. A.: The Curious Case of the Hydrated Proton, Account. Chem. Res., 45, 101–109, https://doi.org/10.1021/ar200140h, 2012.

Kreidenweis, S. and Asa-Awuku, A.: 5.13 – Aerosol Hygroscopicity: Particle Water Content and Its Role in Atmospheric Processes, in: Treatise on Geochemistry, edited by: Holland, H. D. and Turekian, K. K., Elsevier, Oxford, second edition edn., 331–361, ISBN 978-0-08-098300-4, https://doi.org/10.1016/B978-0-08-095975-7.00418-6, 2014.

Kuang, Y., Xu, W., Tao, J., Ma, N., Zhao, C., and Shao, M.: A Review on Laboratory Studies and Field Measurements of Atmospheric Organic Aerosol Hygroscopicity and Its Parameterization Based on Oxidation Levels, Current Pollut. Rep., 6, 410–424, https://doi.org/10.1007/s40726-020-00164-2, 2020.

Lee, H. D., Morris, H. S., Laskina, O., Sultana, C. M., Lee, C., Jayarathne, T., Cox, J. L., Wang, X., Hasenecz, E. S., DeMott, P. J., Bertram, T. H., Cappa, C. D., Stone, E. A., Prather, K. A., Grassian, V. H., and Tivanski, A. V.: Organic Enrichment, Physical Phase State, and Surface Tension Depression of Nascent Core–Shell Sea Spray Aerosols during Two Phytoplankton Blooms, ACS Earth Space Chem., 4, 650–660, https://doi.org/10.1021/acsearthspacechem.0c00032, 2020.

Leng, C.-B., Pang, S.-F., Zhang, Y., Cai, C., Liu, Y., and Zhang, Y.-H.: Vacuum FTIR Observation on the Dynamic Hygroscopicity of Aerosols under Pulsed Relative Humidity, Environ. Sci. Technol., 49, 9107–9115, https://doi.org/10.1021/acs.est.5b01218, 2015.

Li, W., Teng, X., Chen, X., Liu, L., Xu, L., Zhang, J., Wang, Y., Zhang, Y., and Shi, Z.: Organic Coating Reduces Hygroscopic Growth of Phase-Separated Aerosol Particles, Environ. Sci. Technol., 55, 16339–16346, https://doi.org/10.1021/acs.est.1c05901, 2021.

Liang, Z., Chu, Y., Gen, M., and Chan, C. K.: Single-particle Raman spectroscopy for studying physical and chemical processes of atmospheric particles, Atmos. Chem. Phys., 22, 3017–3044, https://doi.org/10.5194/acp-22-3017-2022, 2022.

Lienhard, D. M., Huisman, A. J., Krieger, U. K., Rudich, Y., Marcolli, C., Luo, B. P., Bones, D. L., Reid, J. P., Lambe, A. T., Canagaratna, M. R., Davidovits, P., Onasch, T. B., Worsnop, D. R., Steimer, S. S., Koop, T., and Peter, T.: Viscous organic aerosol particles in the upper troposphere: diffusivity-controlled water uptake and ice nucleation?, Atmos. Chem. Phys., 15, 13599–13613, https://doi.org/10.5194/acp-15-13599-2015, 2015.

Losey, D. J., Parker, R. G., and Freedman, M. A.: pH Dependence of Liquid–Liquid Phase Separation in Organic Aerosol, J. Phys. Chem. Lett. 7, 3861–3865, https://doi.org/10.1021/acs.jpclett.6b01621, 2016.

Losey, D. J., Ott, E.-J. E., and Freedman, M. A.: Effects of High Acidity on Phase Transitions of an Organic Aerosol, J. Phys. Chem. A, 122, 3819–3828, https://doi.org/10.1021/acs.jpca.8b00399, 2018.

Lv, X.-J., Chen, Z., Ma, J.-B., and Zhang, Y.-H.: Evaporation of mixed citric acid/$(NH_4)2SO_4/H_2O$ particles: Volatility of organic aerosol by using optical tweezers, Spectrochim. Ac. Pt. A, 226, 117552, https://doi.org/10.1016/j.saa.2019.117552, 2020.

Ma, S., Chen, Z., Pang, S., and Zhang, Y.: Observations on hygroscopic growth and phase transitions of mixed 1, 2, 6-hexanetriol/$(NH_4)2SO_4$ particles: investigation of the liquid–liquid phase separation (LLPS) dynamic process and mechanism and secondary LLPS during the dehumidification, Atmos. Chem. Phys., 21, 9705–9717, https://doi.org/10.5194/acp-21-9705-2021, 2021.

Maclean, A. M., Smith, N. R., Li, Y., Huang, Y., Hettiyadura, A. P. S., Crescenzo, G. V., Shiraiwa, M., Laskin, A., Nizkorodov, S. A., and Bertram, A. K.: Humidity-Dependent Viscosity of Secondary Organic Aerosol from Ozonolysis of β-Caryophyllene: Measurements, Predictions, and Implications, ACS Earth Space Chem., 5, 305–318, https://doi.org/10.1021/acsearthspacechem.0c00296, 2021.

Mellouki, A., Wallington, T. J., and Chen, J.: Atmospheric Chemistry of Oxygenated Volatile Organic Compounds: Impacts

on Air Quality and Climate, Chem. Rev., 115, 3984–4014, https://doi.org/10.1021/cr500549n, 2015.

Mikhailov, E. F., Pöhlker, M. L., Reinmuth-Selzle, K., Vlasenko, S. S., Krüger, O. O., Fröhlich-Nowoisky, J., Pöhlker, C., Ivanova, O. A., Kiselev, A. A., Kremper, L. A., and Pöschl, U.: Water uptake of subpollen aerosol particles: hygroscopic growth, cloud condensation nuclei activation, and liquid–liquid phase separation, Atmos. Chem. Phys., 21, 6999–7022, https://doi.org/10.5194/acp-21-6999-2021, 2021.

Molinero, V. and Goddard, W. A.: Microscopic Mechanism of Water Diffusion in Glucose Glasses, Phys. Rev. Lett., 95, 045 701, https://doi.org/10.1103/PhysRevLett.95.045701, 2005.

Moridnejad, A. and Preston, T. C.: Models of Isotopic Water Diffusion in Spherical Aerosol Particles, J. Phys. Chem. A, 120, 9759–9766, https://doi.org/10.1021/acs.jpca.6b11241, 2016.

Nadler, K. A., Kim, P., Huang, D.-L., Xiong, W., and Continetti, R. E.: Water diffusion measurements of single charged aerosols using H_2O / D_2O isotope exchange and Raman spectroscopy in an electrodynamic balance, Phys. Chem. Chem. Phys., 21, 15062–15071, https://doi.org/10.1039/C8CP07052K, 2019.

Pigot, C. and Hibara, A.: Surface Tension Measurement at the Microscale by Passive Resonance of Capillary Waves, Anal. Chem., 84, 2557–2561, https://doi.org/10.1021/ac3000804, 2012.

Power, R. M., Simpson, S. H., Reid, J. P., and Hudson, A. J.: The transition from liquid to solid-like behaviour in ultrahigh viscosity aerosol particles, Chem. Sci., 4, 2597–2604, https://doi.org/10.1039/C3SC50682G, 2013.

Preston, T. C. and Reid, J. P.: Determining the size and refractive index of microspheres using the mode assignments from Mie resonances, J. Opt. Soc. Am. A, 32, 2210–2217, https://doi.org/10.1364/JOSAA.32.002210, 2015.

Preston, T. C., Davies, J. F., and Wilson, K. R.: The frequency-dependent response of single aerosol particles to vapour phase oscillations and its application in measuring diffusion coefficients, Phys. Chem. Chem. Phys., 19, 3922–3931, https://doi.org/10.1039/C6CP07711K, 2017.

Price, H. C., Murray, B. J., Mattsson, J., O'Sullivan, D., Wilson, T. W., Baustian, K. J., and Benning, L. G.: Quantifying water diffusion in high-viscosity and glassy aqueous solutions using a Raman isotope tracer method, Atmos. Chem. Phys., 14, 3817–3830, https://doi.org/10.5194/acp-14-3817-2014, 2014.

Pye, H. O. T., Murphy, B. N., Xu, L., Ng, N. L., Carlton, A. G., Guo, H., Weber, R., Vasilakos, P., Appel, K. W., Budisulistiorini, S. H., Surratt, J. D., Nenes, A., Hu, W., Jimenez, J. L., Isaacman-VanWertz, G., Misztal, P. K., and Goldstein, A. H.: On the implications of aerosol liquid water and phase separation for organic aerosol mass, Atmos. Chem. Phys., 17, 343–369, https://doi.org/10.5194/acp-17-343-2017, 2017.

Pöhlker, C., Wiedemann, K. T., Sinha, B., Shiraiwa, M., Gunthe, S. S., Smith, M., Su, H., Artaxo, P., Chen, Q., Cheng, Y., Elbert, W., Gilles, M. K., Kilcoyne, A. L. D., Moffet, R. C., Weigand, M., Martin, S. T., Pöschl, U., and Andreae, M. O.: Biogenic Potassium Salt Particles as Seeds for Secondary Organic Aerosol in the Amazon, Science, 337, 1075–1078, https://doi.org/10.1126/science.1223264, 2012.

Renbaum-Wolff, L., Grayson, J. W., Bateman, A. P., Kuwata, M., Sellier, M., Murray, B. J., Shilling, J. E., Martin, S. T., and Bertram, A. K.: Viscosity of α-pinene secondary organic material and implications for particle growth and reactivity, P. Natl. Acad. Sci. USA, 110, 8014–8019, https://doi.org/10.1073/pnas.1219548110, 2013a.

Renbaum-Wolff, L., Grayson, J. W., and Bertram, A. K.: Technical Note: New methodology for measuring viscosities in small volumes characteristic of environmental chamber particle samples, Atmos. Chem. Phys., 13, 791–802, https://doi.org/10.5194/acp-13-791-2013, 2013b.

Richards, D. S., Trobaugh, K. L., Hajek-Herrera, J., Price, C. L., Sheldon, C. S., Davies, J. F., and Davis, R. D.: Ion-molecule interactions enable unexpected phase transitions in organic-inorganic aerosol, Sci. Adv., 6, eabb5643, https://doi.org/10.1126/sciadv.abb5643, 2020.

Riva, M., Chen, Y., Zhang, Y., Lei, Z., Olson, N. E., Boyer, H. C., Narayan, S., Yee, L. D., Green, H. S., Cui, T., Zhang, Z., Baumann, K., Fort, M., Edgerton, E., Budisulistiorini, S. H., Rose, C. A., Ribeiro, I. O., e Oliveira, R. L., dos Santos, E. O., Machado, C. M. D., Szopa, S., Zhao, Y., Alves, E. G., de Sá, S. S., Hu, W., Knipping, E. M., Shaw, S. L., Duvoisin Junior, S., de Souza, R. A. F., Palm, B. B., Jimenez, J.-L., Glasius, M., Goldstein, A. H., Pye, H. O. T., Gold, A., Turpin, B. J., Vizuete, W., Martin, S. T., Thornton, J. A., Dutcher, C. S., Ault, A. P., and Surratt, J. D.: Increasing Isoprene Epoxydiol-to-Inorganic Sulfate Aerosol Ratio Results in Extensive Conversion of Inorganic Sulfate to Organosulfur Forms: Implications for Aerosol Physicochemical Properties, Environ. Sci. Technol., 53, 8682–8694, https://doi.org/10.1021/acs.est.9b01019, pMID: 31335134, 2019.

Rothfuss, N. E. and Petters, M. D.: Influence of Functional Groups on the Viscosity of Organic Aerosol, Environ. Sci. Technol., 51, 271–279, https://doi.org/10.1021/acs.est.6b04478, 2017.

Ruehl, C. R. and Wilson, K. R.: Surface Organic Monolayers Control the Hygroscopic Growth of Submicrometer Particles at High Relative Humidity, The J. Phys. Chem. A, 118, 3952–3966, https://doi.org/10.1021/jp502844g, 2014.

Sastri, S. and Rao, K.: A new group contribution method for predicting viscosity of organic liquids, Chem. Eng. J., 50, 9–25, https://doi.org/10.1016/0300-9467(92)80002-R, 1992.

Shi, X.-M., Wu, F.-M., Jing, B., Wang, N., Xu, L.-L., Pang, S.-F., and Zhang, Y.-H.: Hygroscopicity of internally mixed particles composed of (NH4)2SO4 and citric acid under pulsed RH change, Chemosphere, 188, 532–540, https://doi.org/10.1016/j.chemosphere.2017.09.024, 2017.

Shiraiwa, M. and Pöschl, U.: Mass accommodation and gas–particle partitioning in secondary organic aerosols: dependence on diffusivity, volatility, particle-phase reactions, and penetration depth, Atmos. Chem. Phys., 21, 1565–1580, https://doi.org/10.5194/acp-21-1565-2021, 2021.

Shiraiwa, M., Ammann, M., Koop, T., and Pöschl, U.: Gas uptake and chemical aging of semisolid organic aerosol particles, P. Natl. Acad. Sci. USA, 108, 11003–11008, https://doi.org/10.1073/pnas.1103045108, 2011.

Smith, N. R., Crescenzo, G. V., Huang, Y., Hettiyadura, A. P. S., Siemens, K., Li, Y., Faiola, C. L., Laskin, A., Shiraiwa, M., Bertram, A. K., and Nizkorodov, S. A.: Viscosity and liquid–liquid phase separation in healthy and stressed plant SOA, Environ. Sci.-Atmos., 1, 140–153, https://doi.org/10.1039/D0EA00020E, 2021.

Stewart, D. J., Cai, C., Nayler, J., Preston, T. C., Reid, J. P., Krieger, U. K., Marcolli, C., and Zhang, Y. H.: Liquid–Liquid

Phase Separation in Mixed Organic/Inorganic Single Aqueous Aerosol Droplets, J. Phys. Chem. A, 119, 4177–4190, https://doi.org/10.1021/acs.jpca.5b01658, 2015.

Sullivan, R. C., Boyer-Chelmo, H., Gorkowski, K., and Beydoun, H.: Aerosol Optical Tweezers Elucidate the Chemistry, Acidity, Phase Separations, and Morphology of Atmospheric Microdroplets, Account. Chem. Res., 53, 2498–2509, https://doi.org/10.1021/acs.accounts.0c00407, 2020.

Tang, M., Chan, C. K., Li, Y. J., Su, H., Ma, Q., Wu, Z., Zhang, G., Wang, Z., Ge, M., Hu, M., He, H., and Wang, X.: A review of experimental techniques for aerosol hygroscopicity studies, Atmos. Chem. Phys., 19, 12631–12686, https://doi.org/10.5194/acp-19-12631-2019, 2019.

Titos, G., Cazorla, A., Zieger, P., Andrews, E., Lyamani, H., Granados-Muñoz, M., Olmo, F., and Alados-Arboledas, L.: Effect of hygroscopic growth on the aerosol light-scattering coefficient: A review of measurements, techniques and error sources, Atmos. Environ., 141, 494–507, https://doi.org/10.1016/j.atmosenv.2016.07.021, 2016.

Tong, Y.-K., Fang, T., Wu, Z., Hu, M., and Ye, A.: Characterizing the hygroscopicity and volatility of single levitated aerosol droplets via optical tweezers-Raman spectroscopy, Environ. Sci.-Adv., 1, 781–789, https://doi.org/10.1039/D2VA00175F, 2022a.

Tong, Y.-K., Liu, Y., Meng, X., Wang, J., Zhao, D., Wu, Z., and Ye, A.: The relative humidity-dependent viscosity of single quasi aerosol particles and possible implications for atmospheric aerosol chemistry, Phys. Chem. Chem. Phys., 24, 10514–10523, https://doi.org/10.1039/D2CP00740A, 2022b.

Tong, Y.-K., Meng, X., Zhou, B., Sun, R., Wu, Z., Hu, M., and Ye, A.: Detecting the pH-dependent liquid-liquid phase separation of single levitated aerosol microdroplets via laser tweezers-Raman spectroscopy, Front. Phys., 10, 969921, https://doi.org/10.3389/fphy.2022.969921, 2022c.

Tong, Y.-K., Wu, Z., Hu, M., and Ye, A.: Measurement Report: Water diffusion in single suspended phase-separated aerosols, PKU [data set], https://doi.org/10.18170/DVN/LJMWYV, 2024.

Vaden, T. D., Imre, D., Beránek, J., Shrivastava, M., and Zelenyuk, A.: Evaporation kinetics and phase of laboratory and ambient secondary organic aerosol, P. Natl. Acad. Sci. USA, 108, 2190–2195, https://doi.org/10.1073/pnas.1013391108, 2011.

Vennes, B. and Preston, T. C.: Calculating and fitting morphology-dependent resonances of a spherical particle with a concentric spherical shell, J. Opt. Soc. Am. A, 36, 2089–2103, 2019.

Virtanen, A., Joutsensaari, J., Koop, T., Kannosto, J., Yli-Pirilä, P., Leskinen, J., Mäkelä, J. M., Holopainen, J. K., Pöschl, U., Kulmala, M., Worsnop, D. R., and Laaksonen, A.: An amorphous solid state of biogenic secondary organic aerosol particles, Nature, 467, 824–827, https://doi.org/10.1038/nature09455, 2010.

Wei, H., Vejerano, E. P., Leng, W., Huang, Q., Willner, M. R., Marr, L. C., and Vikesland, P. J.: Aerosol microdroplets exhibit a stable pH gradient, P. Natl. Acad. Sci. USA, 115, 7272–7277, https://doi.org/10.1073/pnas.1720488115, 2018.

You, Y., Renbaum-Wolff, L., Carreras-Sospedra, M., Hanna, S. J., Hiranuma, N., Kamal, S., Smith, M. L., Zhang, X., Weber, R. J., Shilling, J. E., Dabdub, D., Martin, S. T., and Bertram, A. K.: Images reveal that atmospheric particles can undergo liquid-liquid phase separations, P. Natl. Acad. Sci. USA, 109, 13188–13193, https://doi.org/10.1073/pnas.1206414109, 2012.

You, Y., Smith, M. L., Song, M., Martin, S. T., and Bertram, A. K.: Liquid–liquid phase separation in atmospherically relevant particles consisting of organic species and inorganic salts, Int. Rev. Phys. Chem., 33, 43–77, https://doi.org/10.1080/0144235X.2014.890786, 2014.

Yu, H., Li, W., Zhang, Y., Tunved, P., Dall'Osto, M., Shen, X., Sun, J., Zhang, X., Zhang, J., and Shi, Z.: Organic coating on sulfate and soot particles during late summer in the Svalbard Archipelago, Atmos. Chem. Phys., 19, 10433–10446, https://doi.org/10.5194/acp-19-10433-2019, 2019.

Zawadowicz, M. A., Proud, S. R., Seppalainen, S. S., and Cziczo, D. J.: Hygroscopic and phase separation properties of ammonium sulfate/organics/water ternary solutions, Atmos. Chem. Phys., 15, 8975–8986, https://doi.org/10.5194/acp-15-8975-2015, 2015.

Zhang, Y., Chen, Y., Lambe, A. T., Olson, N. E., Lei, Z., Craig, R. L., Zhang, Z., Gold, A., Onasch, T. B., Jayne, J. T., Worsnop, D. R., Gaston, C. J., Thornton, J. A., Vizuete, W., Ault, A. P., and Surratt, J. D.: Effect of the Aerosol-Phase State on Secondary Organic Aerosol Formation from the Reactive Uptake of Isoprene-Derived Epoxydiols (IEPOX), Environ. Sci. Technol. Lett., 5, 167–174, https://doi.org/10.1021/acs.estlett.8b00044, 2018.

Zhang, Y., Chen, Y., Lei, Z., Olson, N. E., Riva, M., Koss, A. R., Zhang, Z., Gold, A., Jayne, J. T., Worsnop, D. R., Onasch, T. B., Kroll, J. H., Turpin, B. J., Ault, A. P., and Surratt, J. D.: Joint Impacts of Acidity and Viscosity on the Formation of Secondary Organic Aerosol from Isoprene Epoxydiols (IEPOX) in Phase Separated Particles, ACS Earth Space Chem., 3, 2646–2658, https://doi.org/10.1021/acsearthspacechem.9b00209, 2019.

Zhou, Q., Pang, S.-F., Wang, Y., Ma, J.-B., and Zhang, Y.-H.: Confocal Raman Studies of the Evolution of the Physical State of Mixed Phthalic Acid/Ammonium Sulfate Aerosol Droplets and the Effect of Substrates, J. Phys. Chem. B, 118, 6198–6205, https://doi.org/10.1021/jp5004598, 2014.

Zhou, S., Hwang, B. C. H., Lakey, P. S. J., Zuend, A., Abbatt, J. P. D., and Shiraiwa, M.: Multiphase reactivity of polycyclic aromatic hydrocarbons is driven by phase separation and diffusion limitations, P. Natl. Acad. Sci. USA, 116, 11658–11663, https://doi.org/10.1073/pnas.1902517116, 2019.

Zobrist, B., Marcolli, C., Pedernera, D. A., and Koop, T.: Do atmospheric aerosols form glasses?, Atmos. Chem. Phys., 8, 5221–5244, https://doi.org/10.5194/acp-8-5221-2008, 2008.

Zuend, A. and Seinfeld, J. H.: Modeling the gas-particle partitioning of secondary organic aerosol: the importance of liquid-liquid phase separation, Atmos. Chem. Phys., 12, 3857–3882, https://doi.org/10.5194/acp-12-3857-2012, 2012.